Journal Name

ARTICLE TYPE

Cite this: DOI: 00.0000/xxxxxxxxxx

Host guest chemistry and supramolecular doping in triphenylamine-based covalent frameworks on Au(111)†

Christian Steiner,[a‡] Lukas Fromm,[b‡] Julian Gebhardt,[b‡¶] Yi Liu,[a‡] Alexander Heidenreich,[c] Natalie Hammer,[c] Andreas Görling,*[b] Milan Kivala,*[d] and Sabine Maier*[a]

Received Date
Accepted Date

DOI: 00.0000/xxxxxxxxxx

The post-synthetic modification of covalent organic frameworks (COFs) *via* host-guest chemistry is an important method to tailor their electronic properties for many applications. Due to the limited structural control in the assembly of two-dimensional surface-supported COFs, supramolecular networks are traditionally used at present for host-guest experiments on surfaces, which lack structural and thermal stability, however. Here, we present a combined scanning tunneling microscopy and density functional theory study to understand the host-guest interaction in triphenylamine-based covalently-linked macrocycles and networks on Au(111). These triphenylamine-based structures feature carbonyl and hydrogen functionalized pores that create preferred adsorption sites for trimesic acid (TMA) and halogen atoms. The binding of the TMA through optimized hydrogen-bond interactions is corroborated by selective adsorption positions within the pores. Band structure calculations reveal that the strong intermolecular charge transfer through the TMA bonding reduces the band gap in the triphenylamine COFs, demonstrating the concept of supramolecular doping by host-guest interactions in surface-supported COFs. Halogen atoms selectively adsorb between two carbonyl groups at Au hollow sites. The mainly dispersive interaction of the halogens with the triphenylamine COF leads to a small downshift of the bands. Most of the halogens change their adsorption position selectively while annealing near the desorption temperature. In conclusion, we demonstrate evidence for supramolecular doping *via* post-synthetic modification and to track chemical reactions in confined space.

1 Introduction

The post-synthetic modification of nanoporous metal-organic (MOF) and covalent organic frameworks (COF) *via* host-guest chemistry has become a versatile strategy in systematically functionalizing molecular materials. It provides unprecedented chemical, structural, and electronic tunability of the organic framework's properties for applications in various research areas such as separation techniques, catalysis, and sensor devices.[1,2] On metal surfaces, diverse porous molecular architectures with well-defined geometry and size have been obtained in high structural quality to capture molecular guests.[3–6] Most of these porous nanostructures are supramolecular and rely on non-covalent interactions. The reversible nature of the non-covalent interaction facilitates the formation of nearly defect-free, long-range ordered networks; however, at the expense of alterations in structure and pore sizes by the inclusion of guest molecules.[7,8] In contrast, covalently-linked porous networks may offer new opportunities for host-guest chemistry on surfaces due to their higher structural stability leading to robustness against thermal degradation. In particular, the improved thermal stability allows for studying chemical reactions in confined space at elevated temperatures for catalytic applications. Furthermore, host-guest experiments can be applied to tune the electronic properties and band structure of covalently-linked networks and provide interesting insights into

[a] *Department of Physics, Friedrich-Alexander Universität Erlangen-Nürnberg, Erlangen, Germany; E-mail: sabine.maier@fau.de*

[b] *Chair of Theoretical Chemistry, Department of Chemistry and Pharmacy, Friedrich-Alexander Universität Erlangen-Nürnberg, Erlangen, Germany; E-mail: andreas.goerling@fau.de*

[c] *Chair of Organic Chemistry I, Department of Chemistry and Pharmacy, Friedrich-Alexander Universität Erlangen-Nürnberg, Erlangen, Germany.*

[d] *Organisch-Chemisches Institut & Centre for Advanced Materials, Ruprecht-Karls-Universität Heidelberg, Heidelberg, Germany;*
E-mail: milan.kivala@oci.uni-heidelberg.de

† Electronic Supplementary Information (ESI) available: Additional STM Data and DFT calculations. See DOI: 00.0000/00000000.

‡ These authors contributed equally to this work.

¶ Present adress: Fraunhofer Institute for Mechanics of Materials IWM, 79108 Freiburg, Germany.

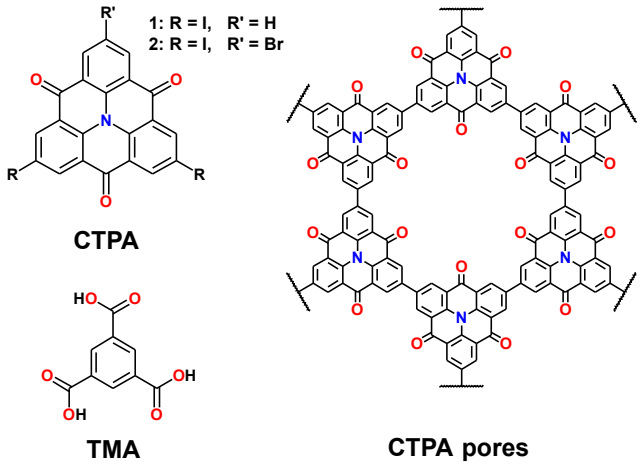

Fig. 1 Chemical structure of the used CTPA1 and CTPA2 that create macrocycles and 2D networks with carbonyl-functionalized pores, respectively, after covalent-bond formation *via* on-surface Ullmann-type reactions. TMA was used as guest molecule.

the concept of supramolecular doping.

The host-guest chemistry in two-dimensional COFs was until now mostly explored at the solid-liquid interface,[9–12] where dynamic covalent chemistry offers a solution to obtain single-layered COFs with small amounts of defects and high surface coverage.[10,13,14]. While there are only a few low-temperature scanning tunneling microscopy (STM) studies in ultra-high vacuum,[15–17] which might relate to the irreversible nature of the covalent bond and the difficulties to obtain long-range order.[18–22] Moreover, mostly carbon-based two-dimensional (2D) porous networks have been studied to avoid competing interactions among the functional groups during the coupling reaction.[19,20,23–25] However, there is no inherent limitation with suitable precursor design to fabricate more complex 2D polymers that feature functionalized pores.[21,26–28] The functional groups facing the pores lay the foundation to bind molecules selectively in the pores.

Herein, halogen-substituted carbonyl-bridged triphenylamines (CTPA) (see Figure 1) on Au(111) are employed to construct macrocycles and nanoporous covalent 2D networks through Ullmann-type reactions.[29] The pores of both, the macrocycles and 2D polymers built from CTPA1 and CTPA2, respectively, have exceptional structural, chemical, and electronic properties: The pore diameter of 1.18 nm between opposite carbonyls is large enough to host small molecules, which can be anchored by the H and O groups providing alternating hydrogen bond donor and acceptor sites in the nanocavity. In addition, the lowest unoccupied orbital faces towards the pore (see Figure S3),[29] which might interact with weakly bonded atoms or molecules trapped in the pores. The host-guest chemistry and changes in the electronic structure based on weakly interacting halogen atoms and hydrogen bonding trimesic acid (TMA) in the carbonyl-functionalized CTPA pores will be discussed by scanning tunneling microscopy experiments in combination with density-functional theory (DFT).

2 Results and discussion

The self-assembled covalent CTPA macrocycles shown in Figure 2 were synthesized from six CTPA1 molecules each *via* a surface-assisted Ullmann-type coupling reaction activated by annealing to 540 K on Au(111) (see Figure S1).[29] We note that at these temperatures, iodine is mostly desorbed and their pores are empty. Both covalently-linked macrocycles and chains are present on the surface; however, for the co-adsorption experiments, we only focus on the macrocycles. In a second step, TMA was deposited at submonolayer coverage (≈ 0.23 ML) at 300 K. We observe that TMA is successfully incorporated into the macrocycle pores with a yield of about 80 % of filled macrocycles as determined from STM overview images. Excess TMA self-assembles around the CTPA structures in an H-bonded honeycomb network, see Figure 2a and Figure S2.[30,31] The adsorbed TMA monomers in the pore of the macrocycles appear as triangles in STM images. The TMA triangles are oriented such that the TMA forms hydrogen bonds to three carbonyl groups of the host pores; see the overlaid structural model as a guide to the eye in Figure 2d. Due to the six-fold symmetry of the CTPA macrocycles and the three-fold symmetry of the TMA, two possible orientations of TMA within pores are expected. This is consistent with the observation of upwards and downwards pointing triangles in Figure 2b. Further, the high-resolution STM image in Figure 2c reveals an off-centered adsorption position of the TMA within the pore, which is reflected by varying distances of 0.98 ± 0.04 nm to 1.08 ± 0.04 nm

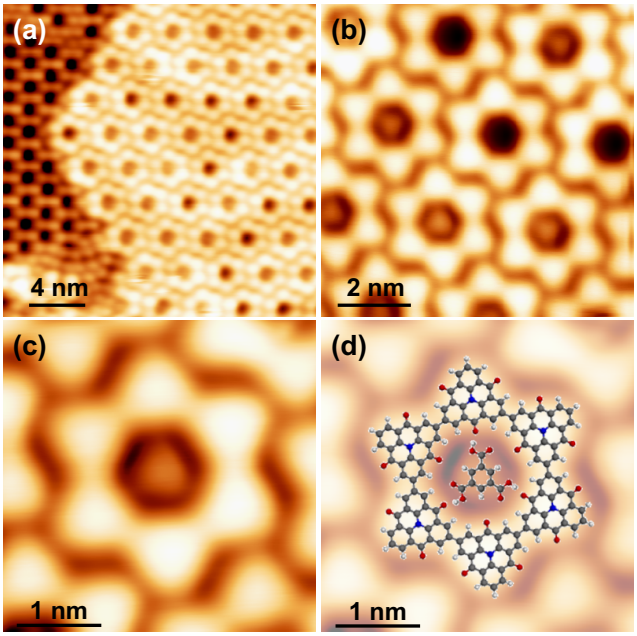

Fig. 2 Host-guest experiments of TMA in CTPA macrocycles on Au(111). (a) STM image of CTPA macrocycles (right) surrounded by H-bonded honeycomb TMA networks (left). (b) STM image showing the two adsorption configurations of the TMA molecules (upward/downward pointing triangles) in the pores. (c-d) High-resolution STM image and overlaid model as a guide to the eye that demonstrates an asymmetric adsorption geometry of the H-bonded TMA molecule in the pore. STM parameters: (a) I=50 pA, V=-1.1 V; (b) I=190 pA, V=-250 mV; (c) I=390 pA, V=340 mV.

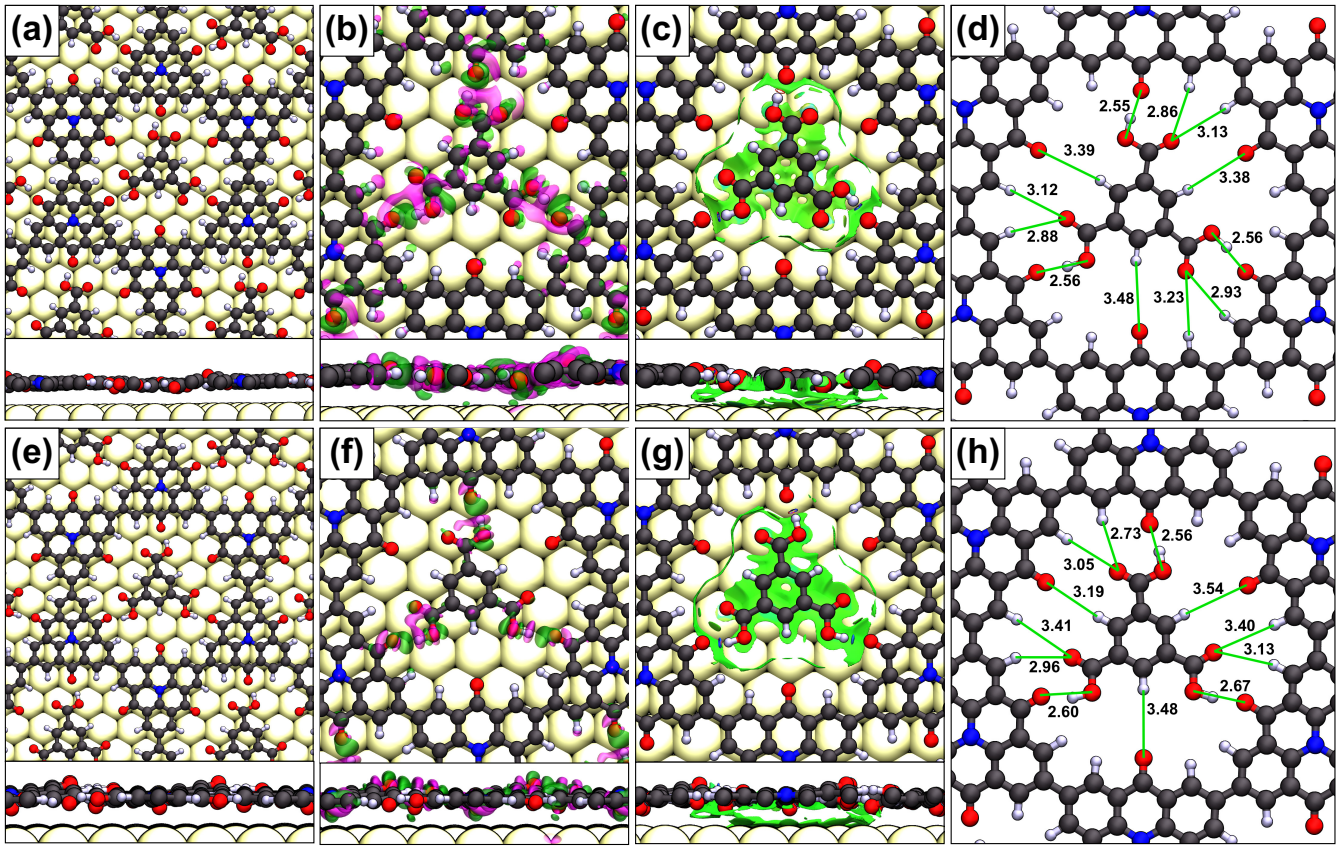

Fig. 3 DFT-optimized (PBE+D3) adsorption structures of a TMA in a CTPA pore on Au(111): (a-d) symmetric conformation, (e-h) asymmetric conformation, (a,e) geometries with bond lengths indicated in Å (d, h; surface is omitted for clarity), (b, f) with the charge density difference showing the TMA and CTPA interaction (charge depletion in purple and charge accumulation in green), and (c, g) the visualization of non-covalent interaction by the reduced density gradient.

between the center of the TMA and the CTPA units' cores (the nitrogen atom). Since the lateral shift is observed in different directions, tip artifacts are unlikely and the asymmetry might be related to the optimization of hydrogen bonds in the slightly oversized pore.

To gain further insight into the adsorption arrangement of TMA molecules in the CTPA pores and the involved interactions, we performed DFT[32,33] calculations using PBE+D3, see Figure 3. DFT calculations for the CTPA structures on Au(111) have been previously reported,[29] therefore, we focus here on the adsorption and interaction of the TMA in the pore of the 2D CTPA network on Au(111). We studied two conformations of the TMA within the pore of the 2D CTPA network: a three-fold symmetric (C_{3h}) and a low symmetry (C_s) conformation, which is obtained by rotating two of the carboxylic acid groups of the symmetric structure (see Figure 3). The symmetric conformation has an adsorption energy of -2.31 eV per TMA in the CTPA network on Au and is by 0.07 eV only slightly more stable than the asymmetric conformation. The largest fraction of the adsorption energy can be attributed to van der Waals interactions of TMA with the surface and the network ($E_{\mathrm{VDW}} = 1.89$ eV). The binding energy $E_{bind} = E_{(\mathrm{CTPA+TMA})_{Au}} - E_{\mathrm{CTPA}_{Au}} - E_{\mathrm{TMA}_{Au}} + E_{Au}$ of the TMA, which quantifies the interaction with the CTPA network, is 0.97 eV. Because of the small energy difference of the two considered arrangements and a high barrier for proton hopping of about 0.9 eV or 0.4 eV for the rotation of the COOH group (from Nudged elastic band calculations), we have to assume that the TMA molecules are statistically distributed in different geometries inside the pores.

To compare the observed asymmetry in the STM data with the DFT results, we measured the variations in the distance of the TMA's center to the surrounding CTPA units' cores (the nitrogen atom). The distance in the optimized DFT structure of the symmetric TMA varies between 9.96 Å and 10.09 Å, revealing a very slight asymmetry. The distances of the asymmetric geometry lie in the range of 9.79 Å and 10.25 Å. The asymmetric arrangement of the COOH groups due to the optimization of the hydrogen bonds leads to unequal COOH···OC bonds and to an overall off-centered adsorption position. Since we did not regard the surface reconstruction of the Au surface and considered only one common surface unit cell for the CTPA network and the Au surface a further off-centered position of the TMA in the pores can be expected. Therefore the resulting variations (0.45 Å in the asymmetric case) reflect well the observed changes in the distances between the center of the TMA and the CTPA unit of 1.0 ± 0.6 Å in the STM. The observed COOH···OC bond lengths of 2.55-2.67 Å lie in the typical range for hydrogen bond distances

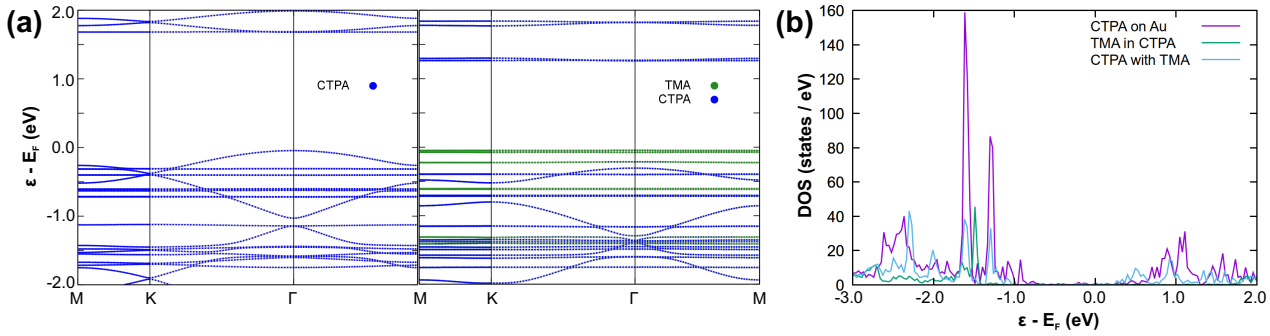

Fig. 4 Supramolecular doping of CTPA networks by the post-synthetic modification *via* TMA adsorption. (a) Calculated band structures of the of CTPA network without (left) and with (right) coadsorbed TMA. The corresponding local density of states maps are shown in Figure S3. (b) Density of states for the CTPA network on Au(111) (purple) and for the CTPA with coadsorbed TMA (green for the TMA and blue for the CTPA). Both in gas-phase and on the surface, a narrowing of the CTPA's band gap is observed upon adsorption of TMA supporting a supramolecular doping effect.

between carbonyl and carboxyl groups.[34] The small variation of these bond lengths shows that the TMA molecule fits quite well into the pores. If at all, the pores are slightly oversized. Moreover, the macrocycle and the incorporated TMA remain mostly planar apart from an out-of-plane distortion of the oxygen atoms of the pores that are interacting with the COOH groups of the TMA.

In addition, we calculated the charge density difference (CDD) plot (Figure 3b,f) that shows charge depletion (purple) from the OH hydrogen atoms, which is accumulated (green) on the oxygen atoms of the network. This non-covalent interaction (NCI) can be further visualized by the reduced density gradient (Figure 3c,g).[35] This shows an attractive interaction between OH hydrogen atoms and oxygen atoms of the network, whereas other non-covalent interactions are weak van der Waals interactions. We note that the differentiation of the shorter H-bonds is subtle in the presented CDD and NCI plots. In conclusion, the host-guest experiments and calculations reveal a strong anchoring of the TMA in the CTPA network, which is dominated by H-bonds of the CTPA carbonyl groups to the COOH groups of the TMA.

We now discuss band structure calculations of the 2D network in order to get more insights on how the adsorption of the TMA affects the electronic structure of the CTPA network. Figure 4a shows the calculated band structure for both the triphenylamine networks in vacuum with and without adsorbed TMA. The direct band gap of the CTPA network at the Γ-point is significantly reduced from 1.72 eV to 1.57 eV upon adsorption of a TMA (with C_{3h} symmetry). Notably, the band gaps computed with PBE+D3 are systematically underestimated by the general gradient approximation, compared to the experimentally observed band gap of the CTPA network of 2.45±0.09 eV.[29] The frontier carbon π-orbitals of the CTPA are arranged in an extended 2D kagome lattice, which leads to an expected electronic structure with Dirac cones at the K-points of the Brillouin zone.[29,36] The Dirac bands become filled due to the central N atom of the triphenylamine. The adsorption of the TMA in the CTPA network opens a sizable band gap for the Dirac cones. The highest occupied molecular orbital (HOMO) of the TMA is located in the band gap of the CTPA network. In conclusion, the TMA adsorption leads to a reduction of the CTPA network's band gap and an opening of the Dirac cones. The narrowing of the band gap is also preserved on the Au(111) as seen in the calculated density of states in Figure 4b. This corroborates the concept of supramolecular doping of the CTPA networks by the post-synthetic modification *via* TMA adsorption. Hence, the presented results demonstrate that the post-synthetic modification *via* host-guest chemistry is a versatile strategy to tune the electronic properties of surface-supported COFs systematically in a reversible way.

In the second part of this study, we focus on weaker supramolecular host-guest interactions in the CTPA pores. We investigated the adsorption position and interaction of halogen atoms, which are available as byproducts in Ullmann-type coupling reactions, as guest species in the nanocavities; see Figure 5. Halogen atoms are chemisorbed on Au(111).[37] Therefore, they interact mostly with the substrate and only weakly with carbon-based nanostructures.[38]

In Figure 5a, STM images of iodines interacting with the carbonyl-functionalized CTPA pores are shown. We reduced the reaction temperature for CTPA1 from 540 K to 473 K to suppress desorption of iodine from the Au(111) surface for these experiments, see Figure S4. At these temperatures, the mobility of CTPA molecules and polymers is limited, resulting in a mix of macrocycles and chains instead of separated well-ordered macrocycle islands, which does not affect the host-guest interactions. The orientation of the macrocycles (axis between opposite carbonyls) varies by ±8° towards the high symmetry axis of the Au lattice and hence the macrocycles do not adsorb strictly commensurate to the Au(111) lattice.

Inside the pores, we find that one, two, or three iodines can adsorb. The CTPA pores lack enough space to accommodate four iodines, as we observed only open pores that contain four iodines (Figure S5). Around the pores, the iodines form extended chains (Figure 5a and Figure S6) interacting *via* iodine–iodine interactions. For one iodine per pore (Figure 5b), the iodine mostly adsorbs in front of the formed C–C bond of the covalently-linked CTPA structures in equal distance between neighboring carbonyl groups. The CTPA pores have six of those adsorption sites near a formed C–C bond; three come with an Au_{hcp} and three with an Au_{fcc} adsorption site for the halogen (see Figure S7). In the STM experiment, three alternate positions are preferred (about 80%), which underlines the preference for one of the hollow sites and

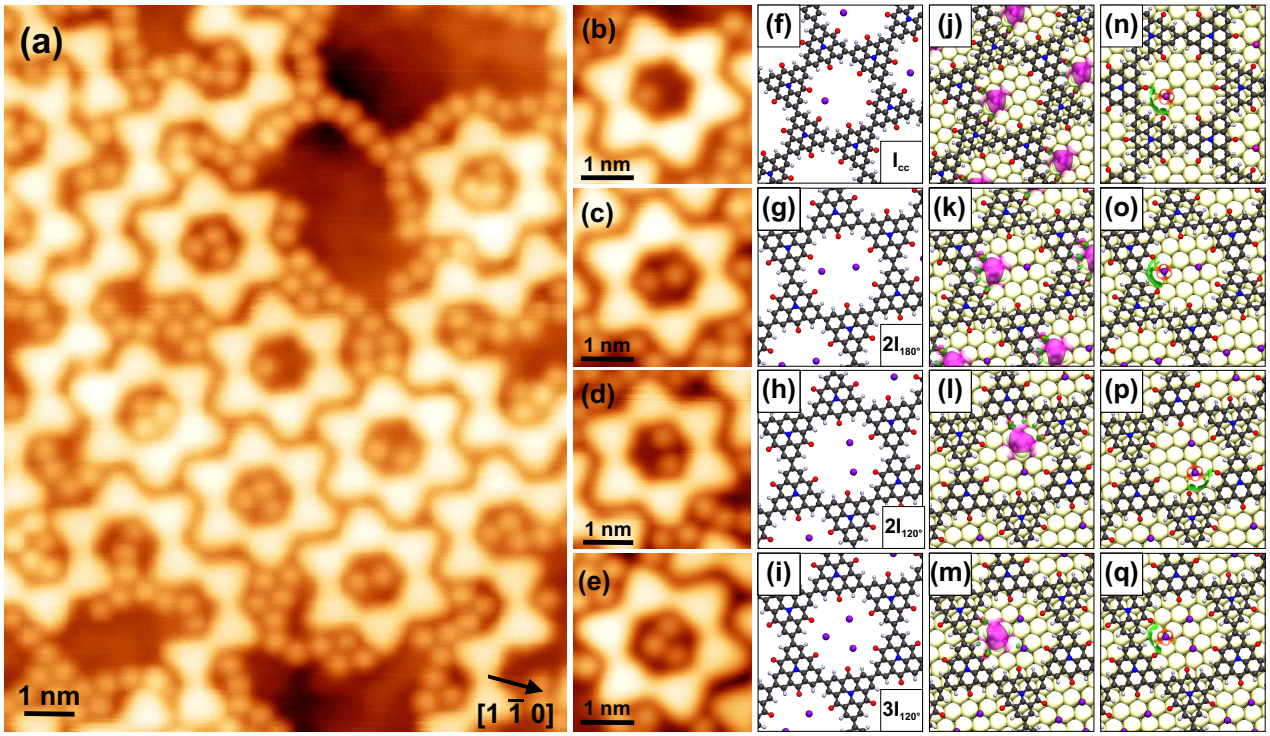

Fig. 5 (a) STM images of the covalently-linked CTPA macrocycles and chains on Au(111) decorated with iodine atoms. (b-e) STM images of macrocycles filled with (b) one, (c-d) two and (e) three iodines, respectively, (f-i) corresponding DFT-optimized adsorption structures on Au(111) (surface is omitted for clarity), (j-m) calculated CDD plots (charge depletion in purple and charge accumulation in green) and (n-q) calculated NCI plots. We note that the $2I_{180°}$ and $3I_{120°}$ arrangements are asymmetric in the STM experiment, which results from an optimization of I···I bonds, while symmetric models were considered in DFT because a common surface unit cell for the CTPA network and the Au surface had to be constructed. STM parameters: (a-e) I=300 pA, V=-0.05 V.

the strong selectivity.

For two and three halogens inside the pores, additionally halogen–halogen interactions influence the adsorption configuration. Two distinct arrangements exist for two iodine atoms in a CTPA pore: a linear arrangement with a 180° angle with respect to the formed C–C bonds ($2I_{180°}$, Figure 5c) and one with a 120° angle ($2I_{120°}$, Figure 5d). The more frequently observed $2I_{180°}$ arrangement (about 70%) has a optimized shorter separation ($d_{I\cdots I}[2I_{180°}] = 4.9 \pm 0.3$ Å vs. $d_{I\cdots I}[2I_{120°}] = 5.7 \pm 0.3$ Å) equal to $\sqrt{3}a_{Au} = 5.0$ Å as observed for extended iodine overlayers forming a commensurate $(\sqrt{3}x\sqrt{3})R30°$ structure on Au(111).[39,40] Three iodines assemble into an asymmetric triangle within a macrocycle-pore (Figure 5d), where one iodine is significantly closer to the center of the pore. The I···I separation decreases to 4.4 ± 0.3 Å, which matches $d_{I\cdots I}$ in iodine overlayers near 0.5 ML coverage.[39,40] Hence, the third iodine is located on the other hollow site as a result of the optimized I···I interaction (Figure S8h). Asymmetric triangles of three iodines are also observed outside of macrocycle pores, which confirms that those assemblies are driven by the I···I interaction (see Figure S8). In summary for two and three halogens, optimizing the I···I is energetically more stable than to maintain for all iodines the same adsorption sites in the CTPA pores in equal distance between neighboring carbonyl groups. We note that iodines in none of the cases adsorb in the center of the pore. Therefore, electron-mediated mutual interactions reinforced by the confinement of surface state electrons in porous molecular networks as previously discussed is not observed in our host-guest experiments.[41,42]

We performed DFT calculations to rationalize the adsorption properties of the halogens and their interactions in the CTPA pores. Iodine preferably adsorbs on hollow over top sites on the clean Au(111), whereas the difference between fcc hollow and hcp hollow sites is negligible (0.04 eV in favor of fcc over hcp, see Table 1). This is comparable to previous DFT results,[43] whereas LEED-IV experiments demonstrated an hcp adsorption.[44] Within the pore, the most stable adsorption site by DFT is the fcc site in front of the formed C–C bond (I_{CC}), in agreement with the STM experiment. However, since iodine shows negligible hollow site preference on Au(111), a simple shift of the structure with respect to the surface would produce an (almost) equally stable hcp site. The halogens have an adsorption height of 2.0 - 2.2 Å and are much closer to the surface than the CTPA network with an adsorption height of 3.4 Å.

The maximal stabilizing effect on the iodine adsorption due to the CTPA network is 0.09-0.13 eV for an fcc and hcp site, respectively. Although this is only a small fraction of the total adsorption energy, this stabilization energy is stronger than adsorption site effects (except the top site destabilization), indicating that the CTPA interaction influence the halogen adsorption pattern. A large fraction of the CTPA influence are dispersive interactions (E_{VDW}=0.11-0.13 eV). The stabilizing effect of the CTPA network results in the preferred adsorption near the network compared

Table 1 DFT adsorption energies (and the fraction of the van der Waals contribution) and structural data of the halogen-CTPA interactions on Au(111). Distances obtained from STM experiments are given in brackets (measurement accuracy ± 0.03 nm). We note that the $2I_{180^\circ}$ and $3I_{120^\circ}$ arrangements are asymmetric in the STM experiment due to the optimization of I···I bonds, while in DFT symmetric models were considered based on the geometric limits from the periodic boundary conditions. The corresponding adsorption geometries for some iodine structures are shown in Figure 5 and for bromine in Figure S8. The unit for all energies is eV and distances nm.

Structure	E_{ads}	E_{VDW}	d_{X-CC}	d_{X-OC}	d_{X-X}
I_{fccH}-free	-2.75	-0.54	-	-	-
I_{hcpH}-free	-2.71	-0.52	-	-	-
I_{bridge}-free	-2.66	-0.51	-	-	-
I_{top}-free	-2.39	-0.46	-	-	-
I_{CC}	-2.84	-0.65	0.59 (0.60)	0.39	-
I_{center}	-2.79	-0.61	0.88	0.60	-
I_{OC}	-2.76	-0.60	0.63	0.32	-
$2I_{120^\circ}$	-2.84	-0.64	0.60 (0.57)	0.38-0.39	0.50(0.57)
$2I_{180^\circ}$	-2.83	-0.63	0.55, 0.65 (0.58, 0.68)	0.35	0.58(0.49)
$3I_{120^\circ}$	-2.83	-0.64	0.54, 0.61, 0.66 (0.57, 0.71)	0.34, 0.38	0.49
Br_{fccH}-free	-2.81	-0.42	-	-	-
Br_{CC}	-2.85	-0.52	0.60	0.39	-
$2Br_{120^\circ}$	-2.84	-0.50	0.60-0.61	0.39	0.49
$3Br_{120^\circ}$	-2.83	-0.49	0.61	0.39	0.49
4Br	-2.80	-0.49	0.53-0.68	0.33-0.52	0.37-0.50

to the pore center I_{center} (0.05 eV). The calculated charge density difference (CDD) plots (Figure 5j-m) confirm that the main bonding interaction of I is with the Au(111) surface, but charge rearrangement is also observed between the network and I. We find interactions with the network oxygen atoms, and somewhat weaker with the hydrogen atoms. This is in line with a charge transfer from iodine to the conduction band (CB), because the valence band (VB) and the CBs of the CTPA network are partially located within the pore (especially CB and CB+1).[29] Therefore, the most stable site in the proximity of the CTPA network is in front of one of the formed C–C bonds. The obtained distances to C–C and C=O bonds are in excellent agreement with experiments, demonstrating good comparability with the STM data, see Table 1. However, the interaction between iodine and the CTPA network is weak and only visible for small iso-density values and dominated by the interaction of iodine to the surface, in line with the discussed dominance of dispersive interactions. This interpretation is also in line with an NCI analysis, which shows strong attractive interactions of iodine only to the surface, whereas non-covalent interactions with the pore are weak (Figure 5).

Similar interactions are observed in DFT calculations for all structures with iodine in front of the formed C–C bond, independent of the specific arrangement or the number of iodine atoms in the pore (see Figure 1). For two iodine atoms in the same pore, both, the $2I_{120^\circ}$ and $2I_{180^\circ}$, are stable with the iodines in the most stable adsorption site (fcc in front of the formed C–C bonds, we rechecked other adsorption sites remain less favorable with respect to the substrate and the polymer). The 120° structure is energetically slightly favorable (0.02 eV/I) due to the smaller I···I separation of 4.97 Å and a small charge rearrangement of neighboring iodine atoms towards each other (Figure 5l). This is consistent with the STM experiments, where we also observed a preference for the smaller I···I separation ($d_{I\cdots I} = 4.9 \pm 0.3$ Å). However, the positioning of the CTPA network on the Au surface in the DFT calculations may slightly differ from the one in the experiment due to the necessity of choosing a common unit cell in the calculation. As a result, the smaller I···I separation is found for the $2I_{120^\circ}$ structure in the calculation whereas it is observed in the $2I_{180^\circ}$ structure in STM. From the results above, we conclude that adding a third iodine atom is most favorable with 120° angles between all iodines. The adsorption energy per halogen in the resulting $3I_{120^\circ}$ structure is slightly decreased 0.02 eV/I. This small effect can be attributed to the high coverage in our calculated model and the resulting weakened substrate effect on each adsorbed halogen. Hence, the adsorption of one to three iodine atoms can be viewed as isoenergetic.

Similarly to the TMA, we investigated the effect of the adsorbed halogens on the electronic structure of the CTPA network. The computed band structures omitting the Au surface, see Figure 6 show no significant effect despite some states from the halogens located near the valence band edge of the CTPA. The weak electronic interaction is expected since the halogens mainly interact with the Au(111) surface. Therefore, we also looked into the density of states for the pristine CTPA network on Au(111) and compared the changes upon adsorption of 1 Br, 1I, and 3I, see Figure 6b. The overall density of states and band gap remain similar, however the halogens lead to a downshift of the bands of less than around 100 meV for 3I and even weaker for one halogen. This is consistent with a previous report about the effect of Br on the electronic properties of polymeric wires.[38]

Next, we studied the adsorption of the halogens in the pores of the covalently-linked triphenylamine networks, which are thermally more stable and hence allow us to make a statistical analysis of the adsorption behavior of the halogen atoms depending on the annealing temperature. In the covalent assembly of the CTPA networks both, iodines and bromines, remain on the surface as a reaction side product. We observed for most halogens the same preferred adsorption position near the formed C–C bond for reac-

tion temperatures below 540 K, only a few (<10%) halogens are found in front of a carbonyl group. This indicates that the adsorption behavior for iodine and bromine is similar. The statistics in Figure 7 indicates that above 540 K, about 50 % of the halogens move to carbonyl sites. We note that the onset temperature for the iodine desorption starts at around 540 K (Figure S4), while the bromines remain on the surface. Thus, we assume the remaining halogens in the network above 540 K are mostly bromines. Choosing atomic halogen radicals as reference states, bromine adsorption is more stable than iodine (0.06 eV/halogen). This trend changes once molecular species are taken into account.[43] Atomic halogens, however, seem to be the more suitable reference, as it has been shown experimentally that these are the desorbing species.[45] We, therefore, are confident that bromine binds stronger to the surface, also leading to somewhat larger adsorption energies within the pore (see Table 1) and higher desorption temperature. Trends observed for iodine are also applicable to bromine: The computed optimal distance to the C–C bonds is identical within the accuracy given in experiments and the resulting distances to C=O bonds are also identical.

Figure 7c-d show detailed STM pictures of the network with halogens adsorbed at both sites, near the C–C bond and near the carbonyl group, respectively. The shift of the halogen adsorption site is observed in macrocycles as well as the 2D networks, which exempts electronic effects of the CTPA structure as an origin. Au adatoms are unlikely to cause these features, because a carbonyl–Au bond is expected to be shorter (0.26 nm).[46] Since the onset temperature of the adsorption site shift correlates with the desorption onset of the iodine and bromine, these are possibly metastable intermediates of those halogens before desorption. Among possible desorption routes are hydrogenated species analogous to the HBr formation previously reported in Ullmann-type reactions.[47,48] This is also supported by our DFT calculations, that predict several isoenergetic adsorption sites (see Tab. SI2). However, the low adsorption energies of ≈ 0.38 eV relative to free molecular HBr indicate that halogenated species may only play a role at final stages of the desorption process. A clear identification of the desorbing species would require an in-depth kinetic analysis to track the desorption process. However, our experiments demonstrate that the covalently-linked framework would enable such future studies and one can track chemical reactions in confined space.

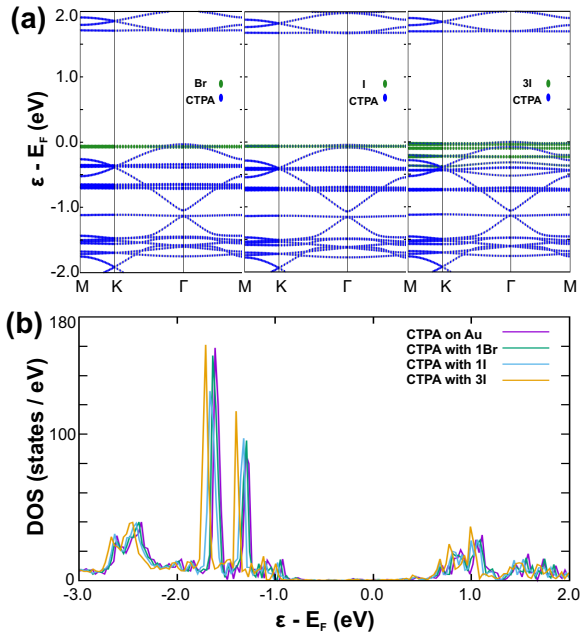

Fig. 6 Electronic structure of the CTPA networks with co-adsorbed halogens. (a) Calculated band structures of the of CTPA network including 1 Br, 1 I, and 3 I in gas-phase. (b) Density of states for the CTPA network on Au(111) (purple) and upon adsorption of halogens.

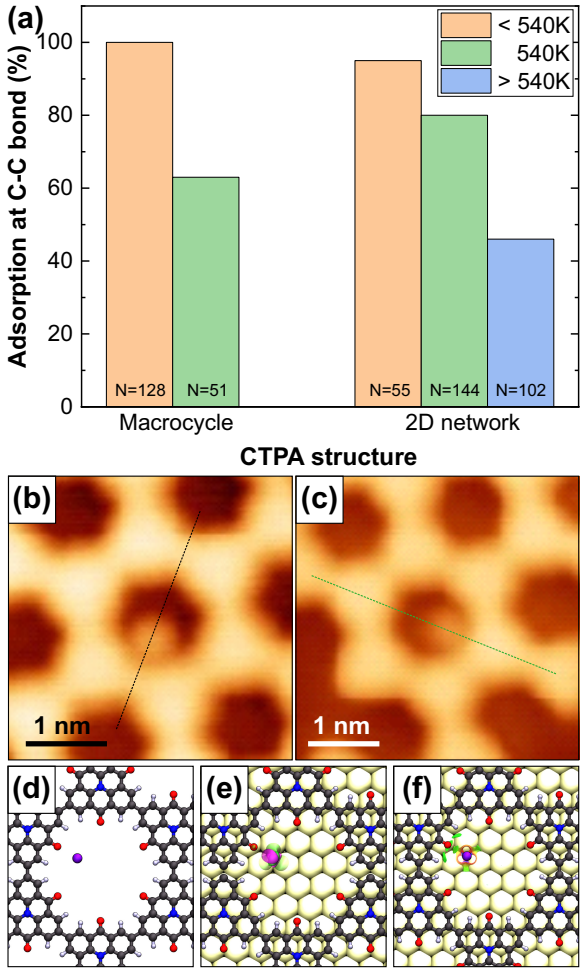

Fig. 7 (a) Statistics on the adsorption sites of the halogens in the CTPA macrocycles and networks after annealing. The percentage of halogens refers to the halogen adsorbed in front of the C–C bond; the rest of the halogens is located in front of carbonyls. (b-c) A halogen adsorbed in front of the (b) C–C bond and (c) the carbonyl group of the CTPA network. The black dashed lines highlight the C–C position, while the green line the carbonyl. STM parameters: (b) I=640 pA and V=0.15 V (c) I=200 pA, V=0.5 V.

3 Experimental Section

3.1 STM experiments

The experiments were performed in a two-chamber UHV system, which operates at a base pressure below $1 \cdot 10^{-10}$ mbar. All STM measurements were conducted with a low-temperature scan-

ning tunneling / atomic force microscope from Scienta-Omicron GmbH in constant-current mode at 4.7 K. The sample is grounded in our experiment and the bias voltage applied to the tip. However, the bias voltages mentioned in the text are given with respect to a grounded tip. A mechanically cut Pt/Ir tip (90% Pt, 10% Ir) was used, which was prepared by field-emission and controlled indentation in the Au(111) surface. The STM images were analyzed using the WSxM software.[49]

A clean Au(111) was prepared by repeated cycles of Ar^+ sputtering (1 kV) followed by annealing at 700 K. The triphenylamine precursors were evaporated with a rate of 0.1 ML min^{-1} from a commercial Knudsen cell (Kentax GmbH) with the crucible held at temperatures between 500 - 550 K and TMA with around 0.05 ML min^{-1} at 415 K, respectively. The rates were determined by a quartz crystal microbalance. The Au(111) substrate was kept a 300 K during the evaporation of the triphenylamine precursors and was subsequently annealed to 473 K to initiate the Ullmann-type coupling reaction. Further details on the on-surface synthesis of CTPA macrocycle and network preparation as well as the synthesis of the triphenylamine precursors are found in Ref. [26]. In a second step, TMA (TCI Chemicals, >98%) was evaporated with the sample kept at room temperature. Both molecules were thoroughly degassed prior to deposition on the surface.

3.2 Computational Details

Closed shell DFT calculations were carried out with the Vienna-ab initio-simulation package[50] employing a plane wave basis set up to a kinetic energy threshold of 415 eV and the projector-augmented wave method[51] for the description of core electrons. The applied Perdew-Burke-Ernzerhof (PBE) exchange-correlation functional[52] was supplied with the D3-correction[53] (using Becke-Johnson damping) to account for dispersive interactions. Energies and geometry optimizations were converged to 10^{-7} eV and forces acting on ions below 0.005 eVÅ, respectively. Free-standing systems in vacuum were computed with 10 Å separating periodic mirror images into the z-direction. Calculations on gold were carried out using a (6×6) replica of an optimized Au(111) (1×1) slab containing three layers, i.e., we are neglecting the reconstruction of the Au(111) surface that occurs in experiments. This simplification is sufficient for a weakly interacting surface at the given level of theory, as proven by the good agreement with experimental results. Therefore, we also did not investigate the structural alignments of the CTPA adsorbate with respect to the substrate in detail. In fact, two different tested structures with the central N atoms over Au(111) fcc-hollow and top sites yield almost isoenergetic adsorption energies (the latter being favored by 0.05 eV per CTPA unit) with identical adsorption distances. During optimizations, only the topmost Au layer was allowed to relax, while the bottom two were fixed at their bulk positions. Due to the metallic character of the system, a first-order Methfessel-Paxton level broadening[54] with a half-width of σ=0.15 eV was used. To account for the finite size of the slab model, a dipole correction[55] was employed into z-direction. Reciprocal space was sampled using a 3×3×1 Monkhorst-Pack grid.[56] Adsorption energies are defined throughout as $E_{\mathrm{ads}} = E(\mathrm{X/Au(111)}) - E(\mathrm{X}) - E(\mathrm{Au(111)})$, i.e., subtracting the energies of the isolated systems from the combined one. Charge-density differences were computed alike by subtracting respective charge densities $\rho^{\mathrm{CDD}} = \rho(\mathrm{X/Au(111)}) - \rho(\mathrm{X}) - \rho(\mathrm{Au(111)})$. The plotted iso-density values for all the adsorbed halogens were set to ± 0.001 electrons/Å^3 and for the TMA to ± 0.005 electrons/Å^3. Non-covalent interactions (NCI) were further analyzed by investigating the reduced-density gradient $s = \frac{1}{2(3\pi^2)^{1/3}} \frac{|\nabla\rho|}{\rho^{4/3}}$ employing the NCI-Plot tool.[35,57] The optimized DFT charge densities were used with standard cut-off parameters of 0.5 a.u. for the iso-surface and ±2.5 a.u. as max./min. values for the color-coding to image the interactions between CTPA and TMA or adsorbed halogens, respectively. The sign of a contribution to the Laplacian of the density along maximal variations (λ_2) can be used to distinguish between attractive (e.g., H-bonding $\lambda < 0$) and repulsive (e.g., steric repulsion $\lambda > 0$) interactions. Thus, a color map from blue over green to red was used to display this information scaled by the density at each point $\mathrm{sgn}(\lambda_2)\rho$. On this scale, weak attractive van der Waals interactions appear green. Climbing-image nudged elastic band calculations were performed to estimate barriers between the two optimized TMA structures via rotation and proton hopping as implemented in VASP according to Henkelman et al.[58,59]

4 Conclusions

In conclusion, this complementary STM and DFT study shows that both TMA molecules and halogen atoms can be trapped selectively at particular sites in the carbonyl-functionalized pores of the covalent CTPA structures through hydrogen bonds or weak van der Waals interactions, respectively. Thereby, an optimization of the hydrogen bond interaction results in a noncentral adsorption of TMA within the pores. Band structure calculations reveal that the strong intermolecular charge transfer through the TMA bonding reduces the band gap in the triphenylamine COFs, demonstrating the concept of supramolecular doping by host-guest interactions in surface-supported COFs.

Iodines and bromines, which mainly bind to the Au(111) - preferably at hollow sites - are stabilized in the pores near the formed C–C bonds. For two and three halogens inside the pores, additionally the adsorption configurations are optimized by halogen–halogen interactions. After annealing to temperatures above 540 K, the halogens change their preferred adsorption sites and move in front of the carbonyls. DFT confirms that this might be related to the formation of intermediate HBr species before desorption. The interaction of the halogens with the CTPA network is too weak to induce a narrowing of the band gap, instead results in a small downshift of the overall density of states.

Hence, our results demonstrate that covalently-linked triphenylamine frameworks offer selective binding sites for weaker, mainly dispersive, and stronger, hydrogen-bonding, interactions. Selective binding is, on the one hand, a crucial finding for future applications as filter membranes or sensing devices. On the other hand, it possibly lays the foundation to push the surface-supported synthesis of covalent porous 2D network by improving the key aspects, the structural quality and scalability, by us-

ing a guest-templated growth as a novel concept. In conclusion, we demonstrate evidence for supramolecular doping *via* post-synthetic modification and chemical reactions in confined space.

Conflicts of interest

There are no conflicts to declare.

Acknowledgements

This work was funded by the German Science Foundation (DFG) through the SFB 953 *Synthetic Carbon Allotropes* (project number 182849149), the FOR 1878 *funCOS - Functional Molecular Structures on Complex Oxide Surfaces*, and GRK 1896 *In situ Microscopy with Electrons, X-rays and Scanning Probes* at the Friedrich-Alexander University Erlangen-Nürnberg. S.M and Y.L. acknowledge the ERC Starting Grant SURFLINK (contract No. 637831). J.G. thanks the DFG for support from the Research Fellowships GE 2827/1-1 and 2827/2-1.

Notes and references

1 K. K. Tanabe and S. M. Cohen, *Chem. Soc. Rev.*, 2011, **40**, 498–519.

2 J. L. Segura, S. Royuela and M. Mar Ramos, *Chem. Soc. Rev.*, 2019, **48**, 3903–3945.

3 J. Teyssandier, S. D. Feyter and K. S. Mali, *Chem. Commun.*, 2016, **52**, 11465–11487.

4 D. Bonifazi, S. Mohnani and A. Llanes-Pallas, *Chem. - A Eur. J.*, 2009, **15**, 7004–7025.

5 T. Kudernac, S. Lei, J. A. A. W. Elemans and S. De Feyter, *Chem. Soc. Rev.*, 2009, **38**, 402–421.

6 J. A. A. W. Elemans, S. Lei and S. De Feyter, *Angew. Chem., Int. Ed.*, 2009, **48**, 7298–7332.

7 X.-H. Kong, K. Deng, Y.-L. Yang, Q.-D. Zeng and C. Wang, *J. Phys. Chem. C*, 2007, **111**, 17382–17387.

8 K. Banerjee, A. Kumar, F. F. Canova, S. Kezilebieke, A. S. Foster and P. Liljeroth, *J. Phys. Chem. C*, 2016, **120**, 8772–8780.

9 D. Cui, J. M. MacLeod, M. Ebrahimi and F. Rosei, *CrystEngComm*, 2017, **19**, 4927–4932.

10 D. Cui, J. M. MacLeod, M. Ebrahimi, D. F. Perepichka and F. Rosei, *Chem. Commun.*, 2015, **51**, 16510–16513.

11 D. Cui, M. Ebrahimi, J. M. Macleod and F. Rosei, *Nano Letters*, 2018, **18**, 7570–7575.

12 J. Sun, X. Zhou and S. Lei, *Chem. Commun.*, 2016, **52**, 8691–8694.

13 J. F. Dienstmaier, A. M. Gigler, A. J. Goetz, P. Knochel, T. Bein, A. Lyapin, S. Reichlmaier, W. M. Heckl and M. Lackinger, *ACS Nano*, 2011, **5**, 9737–9745.

14 R. Tanoue, R. Higuchi, N. Enoki, Y. Miyasato, S. Uemura, N. Kimizuka, A. Z. Stieg, J. K. Gimzewski and M. Kunitake, *ACS Nano*, 2011, **5**, 3923–3929.

15 M. B. Wieland, L. M. A. Perdigao, D. V. Kondratuk, J. N. O'Shea, H. L. Anderson and P. H. Beton, *Chem. Commun.*, 2014, **50**, 7332–7335.

16 C. J. Judd, D. V. Kondratuk, H. L. Anderson and A. Saywell, *Sci. Rep.*, 2019, **9**, 9352.

17 M. O. Blunt, J. C. Russell, N. R. Champness and P. H. Beton, *Chem. Commun.*, 2010, **46**, 7157–7159.

18 S. Maier, in *On-Surface Synthesis of Two-Dimensional Polymers: Rational Design and Electronic Properties*, ed. D. G. de Oteyza and C. Rogero, Springer International Publishing, Cham, 2018, pp. 179–194.

19 J. Eichhorn, D. Nieckarz, O. Ochs, D. Samanta, M. Schmittel, P. J. Szabelski and M. Lackinger, *ACS Nano*, 2014, **8**, 7880–7889.

20 J. Eichhorn, T. Strunskus, A. Rastgoo-Lahrood, D. Samanta, M. Schmittel and M. Lackinger, *Chem. Commun.*, 2014, **50**, 7680–7682.

21 G. Galeotti, F. De Marchi, E. Hamzehpoor, O. MacLean, M. Rajeswara Rao, Y. Chen, L. V. Besteiro, D. Dettmann, L. Ferrari, F. Frezza, P. M. Sheverdyaeva, R. Liu, A. K. Kundu, P. Moras, M. Ebrahimi, M. C. Gallagher, F. Rosei, D. F. Perepichka and G. Contini, *Nat. Mater.*, 2020, **19**, 874–880.

22 S. Whitelam, I. Tamblyn, T. K. Haxton, M. B. Wieland, N. R. Champness, J. P. Garrahan and P. H. Beton, *Phys. Rev. X*, 2014, **4**, 011044.

23 M. Bieri, M. Treier, J. Cai, K. Ait-Mansour, P. Ruffieux, O. Groning, P. Groning, M. Kastler, R. Rieger, X. Feng, K. Mullen and R. Fasel, *Chem. Commun.*, 2009, 6919–6921.

24 C. Moreno, M. Vilas-Varela, B. Kretz, A. Garcia-Lekue, M. V. Costache, M. Paradinas, M. Panighel, G. Ceballos, S. O. Valenzuela, D. Peña and A. Mugarza, *Science*, 2018, **360**, 199–203.

25 P. H. Jacobse, R. D. McCurdy, J. Jiang, D. J. Rizzo, G. Veber, P. Butler, R. Zuzak, S. G. Louie, F. R. Fischer and M. F. Crommie, *J. Am. Chem. Soc.*, 2020, **142**, 13507–13514.

26 T. Faury, F. Dumur, S. Clair, M. Abel, L. Porte and D. Gigmes, *CrystEngComm*, 2013, **15**, 2067.

27 L. Xu, L. Cao, Z. Guo, Z. Zha and S. Lei, *Chem. Commun.*, 2015, **51**, 8664–8667.

28 T. Joshi, C. Chen, H. Li, C. S. Diercks, G. Wang, P. J. Waller, H. Li, J.-L. Bredas, O. M. Yaghi and M. F. Crommie, *Adv. Mater.*, 2019, **31**, 1805941.

29 C. Steiner, J. Gebhardt, M. Ammon, Z. Yang, A. Heidenreich, N. Hammer, A. Görling, M. Kivala and S. Maier, *Nat. Commun.*, 2017, **8**, 14765.

30 Y. Ye, W. Sun, Y. Wang, X. Shao, X. Xu, F. Cheng, J. Li and K. Wu, *J. Phys. Chem. C*, 2007, **111**, 10138–10141.

31 V. Iancu, K.-F. Braun, K. Schouteden and C. Van Haesendonck, *Langmuir*, 2013, **29**, 11593–11599.

32 W. Kohn and L. J. Sham, *Phys. Rev.*, 1965, **140**, 1133–1138.

33 P. Hohenberg and W. Kohn, *Phys. Rev.*, 1964, **136**, B864.

34 T. Steiner, *Angew. Chem., Int. Ed.*, 2002, **41**, 48–76.

35 E. R. Johnson, S. Keinan, P. Mori-Sanchez, J. Contreras-Garcia, A. J. Cohen and W. Yang, *J. Am. Chem. Soc.*, 2010, **132**, 6498–6506.

36 Y. Jing and T. Heine, *J. Am. Chem. Soc.*, 2019, **141**, 743–747.

37 T. A. Baker, C. M. Friend and E. Kaxiras, *J. Am. Chem. Soc.*, 2008, **130**, 3720–3721.

38 G. Vasseur, Y. Fagot-Revurat, M. Sicot, B. Kierren, L. Moreau, D. Malterre, L. Cardenas, G. Galeotti, J. Lipton-Duffin, F. Rosei, M. Di Giovannantonio, G. Contini, P. Le Fèvre, F. Bertran,

L. Liang, V. Meunier and D. F. Perepichka, *Nat. Commun.*, 2016, **7**, 10235.
39 L. Huang, P. Zeppenfeld, S. Horch and G. Comsa, *J. Chem. Phys.*, 1997, **107**, 585–591.
40 S. Cochran and H. Farrell, *Surf. Sci.*, 1980, **95**, 359 – 366.
41 K. Müller, M. Enache and M. Stöhr, *J. Phys. Condens. Matter*, 2016, **28**, 153003.
42 M. Pivetta, G. E. Pacchioni, U. Schlickum, J. V. Barth and H. Brune, *Phys. Rev. Lett.*, 2013, **110**, 086102.
43 J. Björk, F. Hanke and S. Stafström, *J. Am. Chem. Soc.*, 2013, **135**, 5768–5775.
44 Z. V. Zheleva, V. R. Dhanak and G. Held, *Phys. Chem. Chem. Phys.*, 2010, **12**, 10754–10758.
45 G. J. J. Szulczewski and J. M. M. White, *Surf. Sci.*, 1998, **399**, 305–315.
46 S. Irrera and N. H. de Leeuw, *Proc. R. Soc. A Math. Phys. Eng. Sci.*, 2011, **467**, 1959–1969.
47 C. Bronner, J. Björk and P. Tegeder, *J. Phys. Chem. C*, 2015, **119**, 486–493.
48 A. Mairena, M. Baljozovic, M. Kawecki, K. Grenader, M. Wienke, K. Martin, L. Bernard, N. Avarvari, A. Terfort, K.-H. Ernst and C. Wackerlin, *Chem. Sci.*, 2019, **10**, 2998–3004.
49 I. Horcas, R. Fernandez, J. M. Gomez-Rodriguez, J. Colchero, J. Gomez-Herrero and A. M. Baro, *Rev. Sci. Instrum.*, 2007, **78**, 013705.
50 G. Kresse and J. Furthmüller, *Comput. Mater. Sci.*, 1996, **6**, 15–50.
51 P. E. Blöchl, *Phys. Rev. B*, 1994, **50**, 17953.
52 J. P. Perdew, K. Burke and M. Ernzerhof, *Phys. Rev. Lett.*, 1996, **77**, 3865–3868.
53 S. Grimme, J. Antony, S. Ehrlich and H. Krieg, *J. Chem. Phys.*, 2010, **132**, 154104.
54 M. Methfessel and A. T. Paxton, *Phys. Rev. B*, 1989, **40**, 3616–3621.
55 J. Neugebauer and M. Scheffler, *Phys. Rev. B*, 1992, **46**, 16067.
56 H. J. Monkhorst and J. D. Pack, *Phys. Rev. B*, 1976, **13**, 5188–5192.
57 J. Contreras-García, E. R. Johnson, S. Keinan, R. Chaudret, J.-P. Piquemal, D. N. Beratan and W. Yang, *J. Chem. Theory. Comput.*, 2011, **7**, 625–632.
58 G. Henkelman, B. P. Uberuaga and H. Jónsson, *The Journal of Chemical Physics*, 2000, **113**, 9901–9904.
59 G. Henkelman and H. Jónsson, *The Journal of Chemical Physics*, 2000, **113**, 9978–9985.